Design Studies on Mechanically Geared, Magnetically Geared, and Direct Drive Drivetrains for UAM Applications

Thomas Tallerico[1], Jeffryes Chapman[2], and Andrew Smith[3]
NASA Glenn Research Center, Cleveland, OH, 44135

Urban air mobility vehicles require high reliability and high performance electric motor drivetrains. In this paper, a design optimization study is carried out to compare mechanically geared, magnetically geared, and direct drive motor drivetrain topologies' achievable performance in a 100 kW hover power quad rotor propulsor application. Design studies are carried out accounting for a nominal mission profile and assuming constant propulsor rotor RPMs of 400, 1000, 2000, and 3000 RPM. Results show that mechanically geared drives are the lightest at all RPMs but their mass benefit over direct drive and magnetically geared decays with increased rotor RPM. Direct drive is shown to always achieve the highest efficiency due to its lower motor speed resulting in low electrical frequencies. Magnetically geared drivetrains in the initial study are required to provide 50% torque margin and have similar performance to direct drive drivetrains. It is shown that reducing this margin makes magnetically geared drivetrains performance competitive with high efficiency mechanically geared drivetrains and lighter than direct drive drivetrains.

I. Introduction

Urban Air Mobility (UAM) requires high performance electric motor drivetrains to minimize the energy consumption and cost of each flight. One of the fundamental questions in the design of an electric motor drivetrain is whether or not to use a gearbox. Additionally, research groups at NASA [1], Texas A&M [2], and The University of Portland [3] [4] have proposed and developed magnetic gears for electric aircraft propulsion applications. This paper presents a comparison of three electric aircraft drivetrain topologies (Mechanically Geared, Magnetically Geared, and Direct Drive) within the context of a 100 kW hover power quadrotor UAM vehicle propulsor.

Past work by the University of Illinois studied mechanically geared vs direct drive drivetrains topologies for larger fixed wing transport style aircraft [5]. Schweigert et al completed a detailed study on optimum machine speed and gearbox design for electric cars [6]. Neither study targets UAM applications, mission profile considerations, or full propulsion system design (gearbox, inverter, motor, and thermal management system).

In this paper, the UAM motor design tool developed in [7] and [8] is used to compare the different drivetrain topologies. The target mission profile for the design is based on the NASA UAM concept vehicles studied in [9] [10] and [11]. Prior studies by NASA on magnetically geared motors [12] [13] and [14] are used to down select magnetic gear motor topology down to an outer stator magnetically geared motor (OSMGM). All three drive train topologies are optimized for a 100 kW hover power propulsor at 400, 1000, 2000, and 3000 RPM. Results are compared in terms of total propulsor mass and total propulsor mission efficiency. The results of this paper are only for a single set of assumptions, power level, application, and technology and should not be considered generally applicable across the full UAM design space.

Section II of this paper details design methodology and updates to the UAM motor design tool. Section III presents results of the design study. Section IV provides a conclusion summarizing the results.

[1] Aerospace Research Engineer, Rotating and Drives Systems
[2] Aerospace Research Engineer, Systems Analysis
[3] Aerospace Engineer, Thermal Management

II. Design Optimization Methodology

The design tools used in this paper corresponds to updated versions of the UAM motor drivetrain design tool presented in [7]. The two flow diagrams in Figure 1 depict the two versions of the design tool used in this paper, one for motor-based designs and one for OSMGM-based designs. The following sections first detail the updates to the motor-based design tool and then the adaptation of the design tool to OSMGM-based designs.

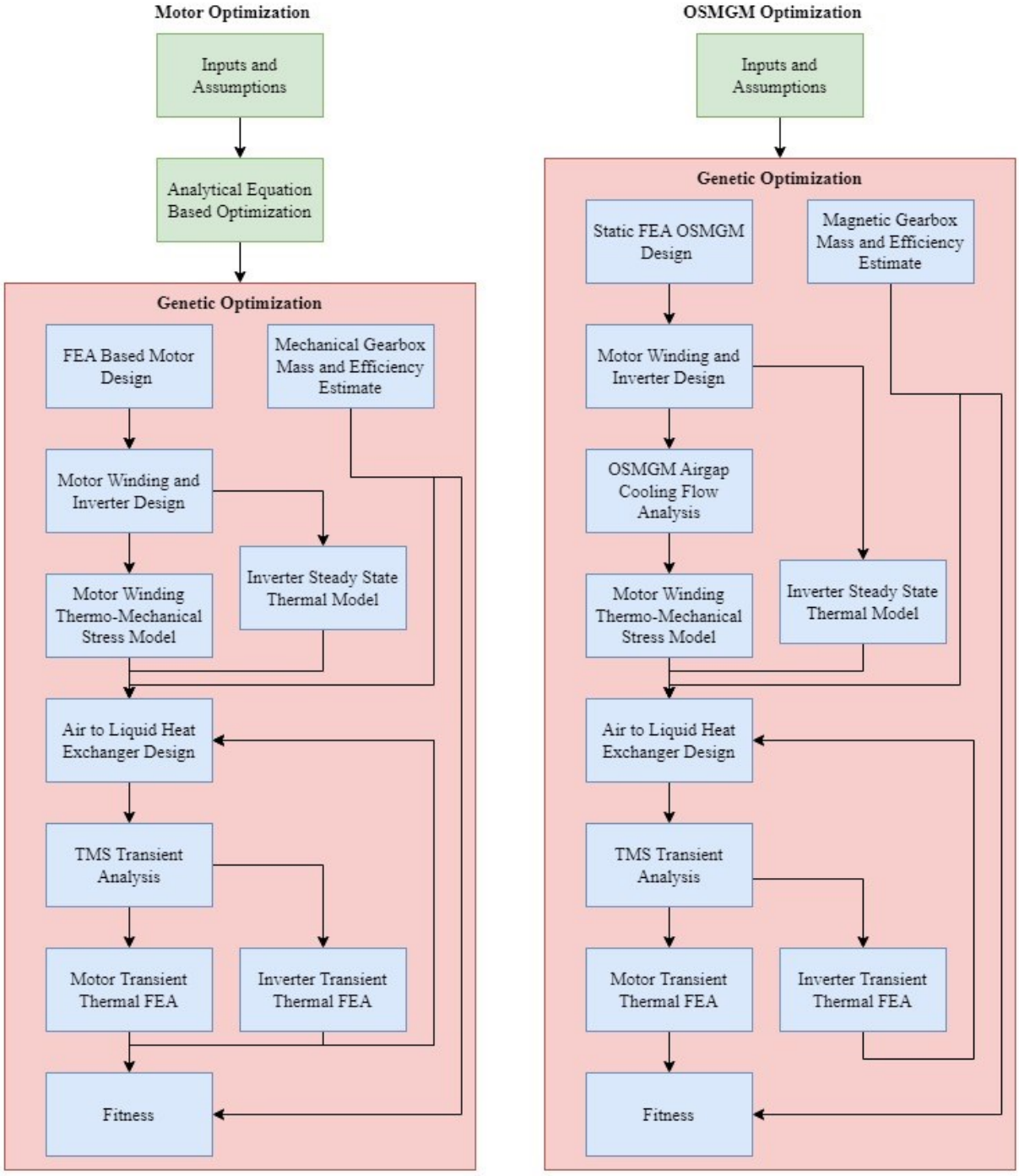

Figure 1 Design Tool Flow Diagrams

A. Updates to Motor Drivetrain Design Tool

1. Analytical Preoptimization

To reduce the computational cost of the detailed finite element analysis (FEA) based optimization, analytical pre-optimizations of gearbox, motor, inverter, and thermal management system (TMS) were incorporated into this version of the motor drivetrain design tool. This analytical optimization uses the preoptimized mechanical gearbox performance curves generated using the method described in [15], the analytical motor model from [8], the analytical inverter design tool discussed in [7] and [16], and HEATSSPY [17] an open source thermal management system design tool based on OPENMDAO. The analytical preoptimizations build a good initial population for the FEA based tool. The FEA based optimization then filters out designs whose performance was overpredicted using analytical equations before completing further optimization of the remaining designs.

2. Mechanical Gear Box Sizing

In [7], gearbox mass and efficiency were assumed to only depend on the gear ratio for a given power and output speed. As an update to the tool, a gearbox specific torque index was added as a genetic optimization variable. Gearbox designs were still pre-generated using the design tool described in [15]. The pareto fronts at each gear ratio analyzed were then used to create a scattered interpolant function with inputs of gear ratio and specific torque index. The specific torque index controls whether at a given gear ratio a high mass, high efficiency design or a low mass, low efficiency design is selected. The result of this update is that the overall mass of the drivetrain in the mechanically geared results do not purely trend with motor mass as they did in [7] and more significantly correlate with gearbox mass.

3. Rotor Loss at Each Mission Point

In past versions of the motor mission profile analysis, rotor magnet and iron loss were assumed to be constant across the entire mission [7] [8]. To make some attempt to account for the effect of stator current on the magnitude of rotor loss, max magnetic field in each component is calculated via static FEA for zero stator current and each mission design point. The difference in max magnetic field for each stator current relative to no stator current is used to scale the rotor and magnet losses calculated using the pseudo time stepping FEA at climb condition. The scaling is completed using

$$Rotor\_Loss_{missionpoint} = Rotor\_Loss_{psuedoFEA} * (\frac{B_{static,mission} - B_{no-current}}{B_{staticclimb} - B_{no-current}})^{\beta}$$

Where $Rotor\_Loss_{missionpoint}$ is the estimated loss at each mission point, $Rotor\_Loss_{psuedoFEA}$ is the rotor loss calculated using pseudo time stepping FEA at climb condition, $B_{static,mission}$ is the max field in a rotor component from static FEA at the mission point, $B_{no-current}$ is the max field in a rotor component from the no stator current static FEA, $B_{staticclimb}$ is the max field in a rotor component from static FEA at the climb mission point, and β is the field depended exponent for the loss in the component (2 for magnet eddy currents and 1.5 for iron loss).

4. TMS Design Flow

In the previous version of the motor drivetrain design tool [7], the TMS liquid-to-air heat exchanger design was completed once before passing the results to the transient thermal model of the motor and if that model resulted in a failure of the design due to thermo-mechanical stress or winding thermochemical life, the design was assigned a fitness of zero. In this updated version of the tool, a failure as a result of either inverter or motor transient thermal FEA results in a redesign of the liquid-to-air heat exchanger with a lower target steady state temperature and another iteration of the transient thermal models unless the target steady state temperature for the fluid has dropped below 50 C.

5. Inverter Transient

To raise the fidelity of the thermal analysis of the inverter in the design tool, a transient mission profile FEA thermal analysis of the inverter was incorporated into the design flow. This allows for more accurate predictions of inverter component temperature over the mission profile at a relatively small computational cost.

B. Adaptation for Direct Drive

For direct drive machines, three changes are made to the design tool. Firstly, the bearing code is changed from the motor bearing code from [8] to the propellor shaft and bearing code from [15] so that both geared and direct drive machines account for the bearings and shafts needed to react the loads of the propellor. Second, the assumed coolant is changed from oil to a 50/50 PGW mixture since there is no gearbox requiring oil lubrication. Third, rotor pole count is not an optimization variable for the direct drive case. Since RPM is assumed to be constant in these studies, electrical frequency is used to define rotor pole count in the optimization.

C. Adaptation to OSMGM design Tool

1. Optimization Variables

For the OSMGM design tool, 12 genetic optimization variables are used. Table 1 lists the variables. Sun gear radius instead of tip speed is used to control the diameter of the gear, because of magnetic gear's high mass sensitivity to radius [18]. Both a second stage concentric magnetic gear (CMG) gear ratio, if applicable, and the OSMGM's gear ratio are used to control the rotational speed of the sun gear and modulator of the OSMGM. Electrical frequency in turn sets the sun gear pole count. Sun magnet, ring magnet, and modulator thickness are all controlled at the top level of the optimization. OSMGM stator mass replaces motor mass since the stack length and mass of the magnetic gear portion of the OSMGM is set by the required torque. Using stator mass as a genetic optimization variable allows the stator to be designed to maximize efficiency and thermal performance within a fitness evaluation. Both ring magnet and sun magnet temperatures are allowed to be optimized by the code. Internal airgap cooling and the added windage losses to maintain magnet temperatures are accounted for as described in Section III B 4.

Table 1 Genetic Optimization Variables for OSMGM Design Tool

Second Stage Gear Ratio	OSMGM Gear Ratio
Sun Gear Radius	Electrical Frequency
Sun Magnet Thickness	Modulator Thickness
Ring Magnet Thickness	OSMGM Stator Mass
Inverter Mass	Ring Magnet Temperature
Sun Magnet Temperature	Coolant Volumetric Flow Rate

2. CMG Gearbox Stage

If a concentric magnetic gear stage is used before the OSMGM in a 2-stage drivetrain, a simple one-dimensional correlation for gearbox mass and efficiency as a function of gear ratio is used to include CMG mass and efficiency in the performance prediction for the drivetrain. A two-dimensional one like the one used for mechanical gearboxes is not used due to the higher mass and higher efficiency of the magnetic gears per Section III-A-2 making it logical to prioritize minimizing the mass of the magnetic gearbox at the cost of efficiency in these design studies.

The data used to create the correlation for gearbox mass and efficiency as a function of gear ratio are generated using a genetic optimization of a concentric magnetic gear. The design flow within the genetic optimization fitness evaluation is based off of the design code used in previous magnetic gear sizing studies [19]. Different from [19], the code makes an approximate efficiency estimate for the gear based on static FEA (Figure 2) and ring gear back iron is included in the geometry of the concentric magnetic gear to allow the use of a metal housing around the gear. The bearings and shafts of the concentric magnetic gear are sized using the code from [15] so that propellor loads and moments are accounted for in both mechanical and magnetic gearbox designs.

The loss estimation methodologies used in [14] and [12] are used to estimate modulator iron, ring gear magnet, ring gear iron, and windage losses. Some estimates of the difference between these loss calculations and loss calculations that used pseudo time stepping FEA can be found in [12] [13] [14]. Sun gear magnetic loss was neglected in past work. As a simple approximation in the paper, sun gear magnet loss is estimated as

$$Sun_{Loss} = Ring_{Loss} * (GR - 1)^2$$

The magnets are assumed to be samarium cobalt operating at 160 C. All magnets are assumed to be composed of 1 mm laminations to suppress eddy current losses in the magnets. In the magnetic simulations of the gears, a 10% reduction is applied to the remanent flux density of the magnets to account for loss of magnet fill due to the use of laminations.

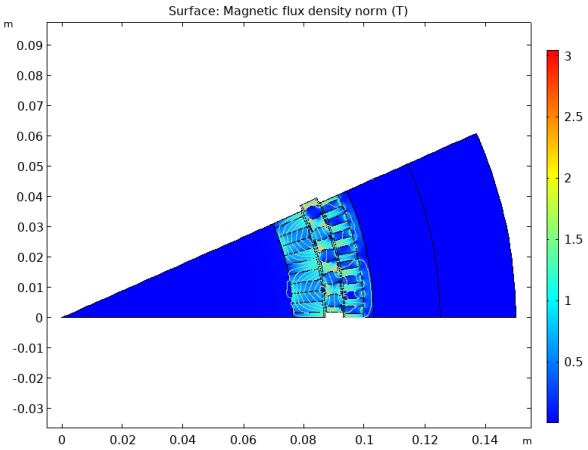

Figure 2 Example CMG Magnetic Simulation Geometry and Result

3. OSMGM Sizing

Static 2D FEA simulations are used to calculate the torque per meter of the magnetic gear portion of the OSMGM and the torque per meter per amp of stator current of the motor portion of the OSMGM. An example geometry and result for this simulation is shown in Figure 3. The torque-per-meter of the gear portion is used to define its stack length based on the required torque. 3D leakage is accounted for in the magnetic gear torque prediction and in the motor torque calculation using a correlation based on the data found in [20] for magnetic gear 2D to 3D torque reductions.

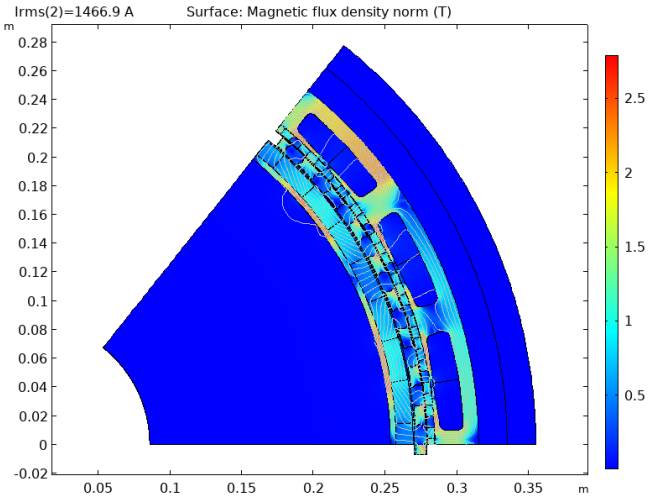

Figure 3 Geometry and Example Result for Static 2D OSMGM FEA

The stator stack length is sized by extrapolating from the 2D FEA the stator and its heat sink performance vs stator radial thickness, stator back iron thickness, stator tooth thickness, and heat sink fin height. Stack length for set combinations of these variables is back calculated such that the stator mass is roughly equal to the stator mass selected by the genetic optimizer for a given fitness evaluation. Losses and an analytical prediction of stator thermal performance are calculated for each case. A stator design is then selected based on maximizing the thermal performance of the OSMGM.

A parametric stator electrical current sweep for the selected geometry is carried out in static 2D FEA. Required stator electrical current for each mission design point is defined. Static FEA is then carried out at each of these set electrical current points to calculate both the fields in all components and the inductance of the stator coil. The field data is used to create magnetic loss estimates for the various components at each mission design point using the methodology from [13]. To capture an estimate of the sun gear iron and magnet loss caused by the ring gear, a static FEA simulation is carried out with the sun gear magnetization set to zero. The field data in the sun magnets and the sun gear back iron from this simulation is used to estimate the losses caused by ring gear magnetic flux. Stator

electrical current caused losses in the sun gear are neglected assuming that the ring gear generates the bulk of the loss given its relative magnetic strength and high electrical frequency relative to the sun gear [18].

4. OSMGM Airgap Cooling Flow

In [14] [13] [12], the modulator of the magnetically geared motor was consistently found to reach high temperatures when high fidelity thermal analysis was completed. To compensate for this and to allow magnet temperature to be an optimization variable, air gap cooling flow was added to the machine designs. A parametric sweep of volumetric flow rates was carried out in 3D thermal FEA to define the required volumetric flow rate of coolant required to maintain target magnet and modulator temperatures in the OSMGM designs. The geometry of this model is shown in Figure 4. Like in [12] and [14], the internal air is modeled as a solid body with high thermal conductivity and thermal contact boundary conditions are used to represent the convective heat transfer between the OSMGM components and the internal air.

From the analysis, magnet, and iron temperatures are extracted as a function of airgap flow and a required volumetric flow rate of air is defined. Windage calculations are completed for this required axial flow rate of air and incorporated into efficiency estimates for the machine. All subsequent thermal simulations of the machine include boundary conditions with heat transfer coefficients corresponding to the required airgap cooling flow rate. Magnet and Iron temperatures are checked after thermal transient FEA to verify that temperature limits for their respective materials have not been exceeded.

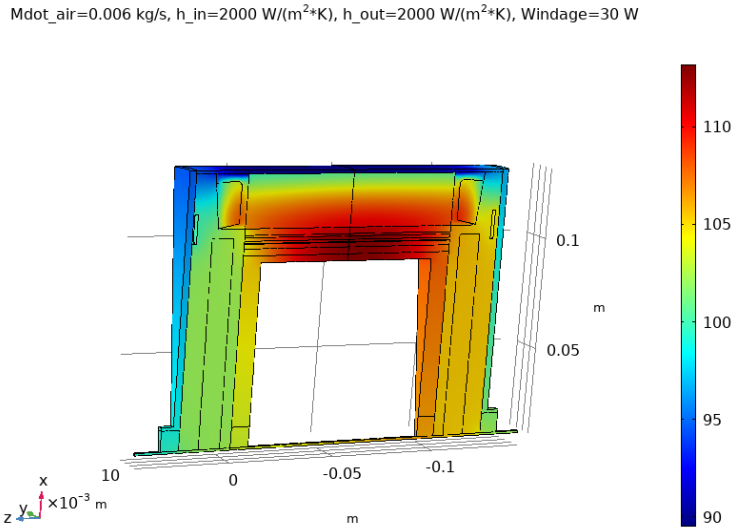

Figure 4 Geometry of Airgap Cooling Flow Simulations and Example Results. Temperature shown in degrees C

III. Results

Design studies were completed for the NASA RVLT six passenger quad rotor reference vehicle. The assumed mission profile for this vehicle is defined in Table 2. This is the same mission as was used in [7] and [8]. Design optimizations are carried out for each drive topology at 400, 1000, 2000, and 3000 RPM. All designs are assumed to operate at constant RPM throughout the mission profile. All magnetic gears are sized for 150% the peak nominal mission power so that slip, and corresponding loss of control can be avoided. 50% margin may be a conservative estimate in the general studies presented here. More complete knowledge of a vehicle and its required control response could raise or lower this margin. Section III-A presents the mechanical gearbox and magnetic gearbox optimization results used in subsequent optimizations of geared drivetrains. Section III-B presents results for full drivetrains at each RPM. Section III-C presents results for reduced airgap and reduced margin magnetically geared drives and a discussion of what would be needed to make the magnetically geared drives competitive with direct drive and mechanically geared drives.

Table 2 Design Mission Profile

Assumed Quadrotor Propulsion Mission Profile		
Mission Segment	**Power (kW)**	**Time (s)**
Hover1 (takeoff 1)	100	40
Climb1	140	240
Cruise1	70	1200
Hover2 (land 1 + takeoff 2)	100	80
Climb2	140	240
Cruise2	70	1200
Hover3 (land 2	100	40
Emergency	133	120

A. Gearbox Results

1. Mechanical Gearboxes

Mechanical gearbox preoptimizations were carried out 400, 100, 2000, and 3000 RPM. In each case the gears were sized for a life of 5000 hours with 99% reliability at peak mission torque (climb condition – 140 kW). Optimizations were carried out for 3 types of gearboxes: 1 stage planetary, 2 stage planetary, and a planetary output stage plus a spur gear input stage. The results of the optimizations are shown in Appendix A. Figures 5 thru 8 show the outputs of the gearbox scattered interpolant functions at each RPM. Minimum gearbox mass is shown to decay with rotor RPM in Figures 5-8 but with marginal returns corresponding to gearbox specific torque decaying with reduced gearbox torque [15] [21]. Gear efficiency at a given motor RPM is shown to increase with propulsor rotor speed due to higher rotor RPM resulting in less load on the gears and lower gear ratios. Gear mass is shown to stay relatively constant at gear ratios greater than 5 in Figures 5-8 due to 2 stage gearboxes becoming optimum at those gear ratios and the second stage being lower mass and having minimum impact on the overall gearbox mass.

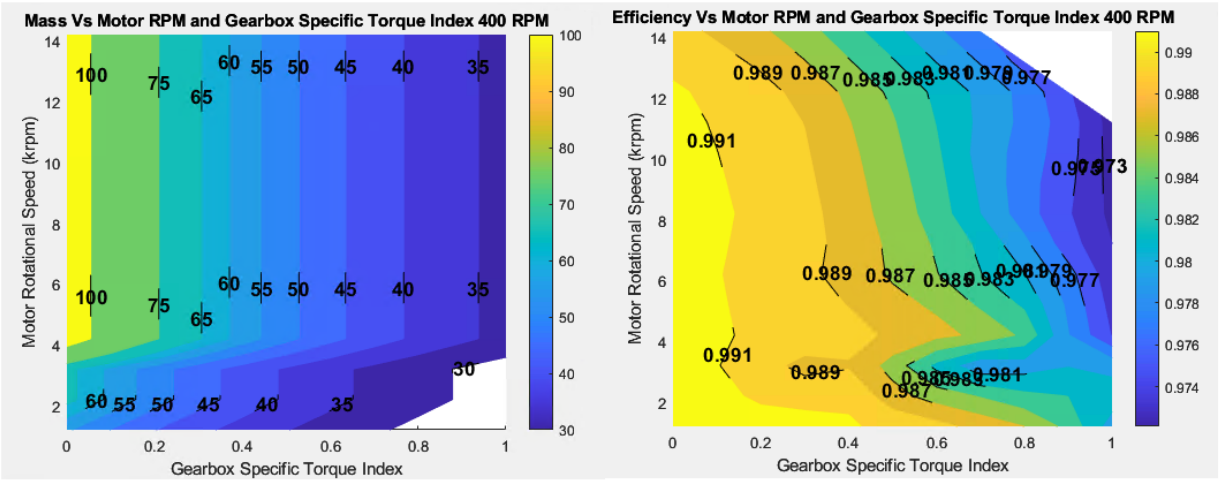

Figure 5 Gearbox scattered interpolant function results for mass and efficiency at 400 rpm

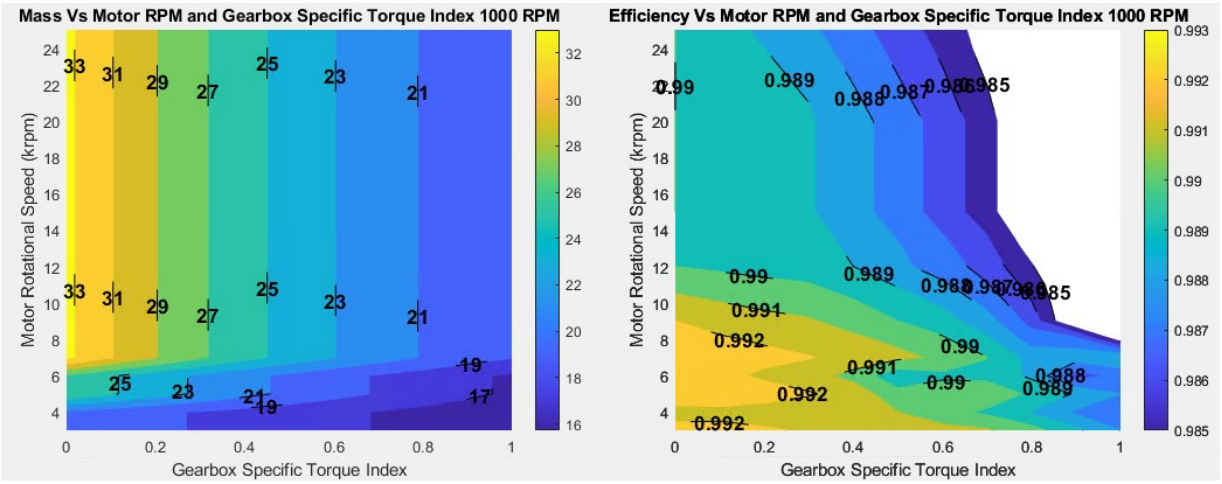

Figure 6 Gearbox scattered interpolant function results for mass and efficiency at 1000 rpm

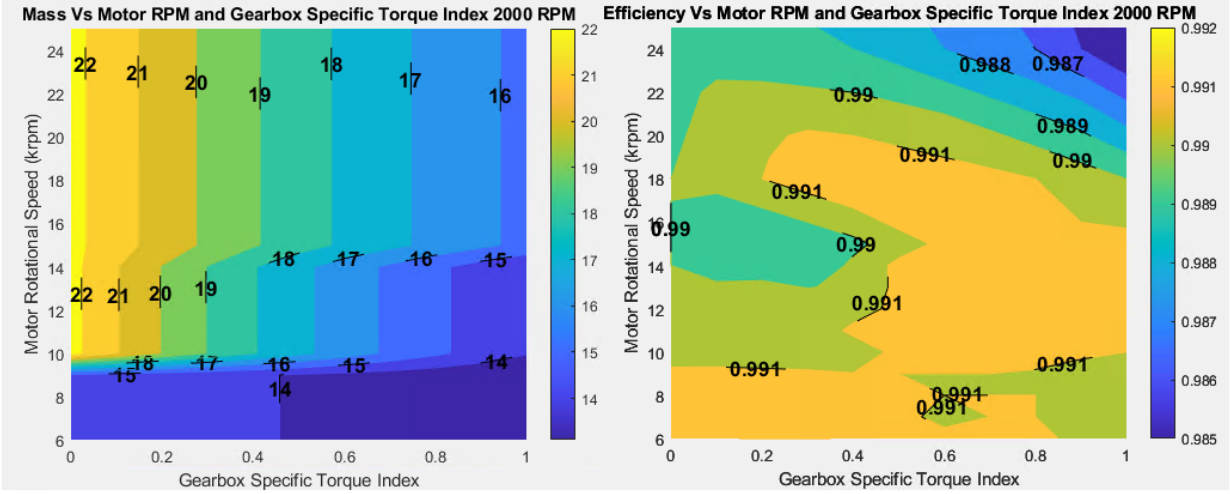

Figure 7 Gearbox scattered interpolant function results for mass and efficiency at 2000 rpm

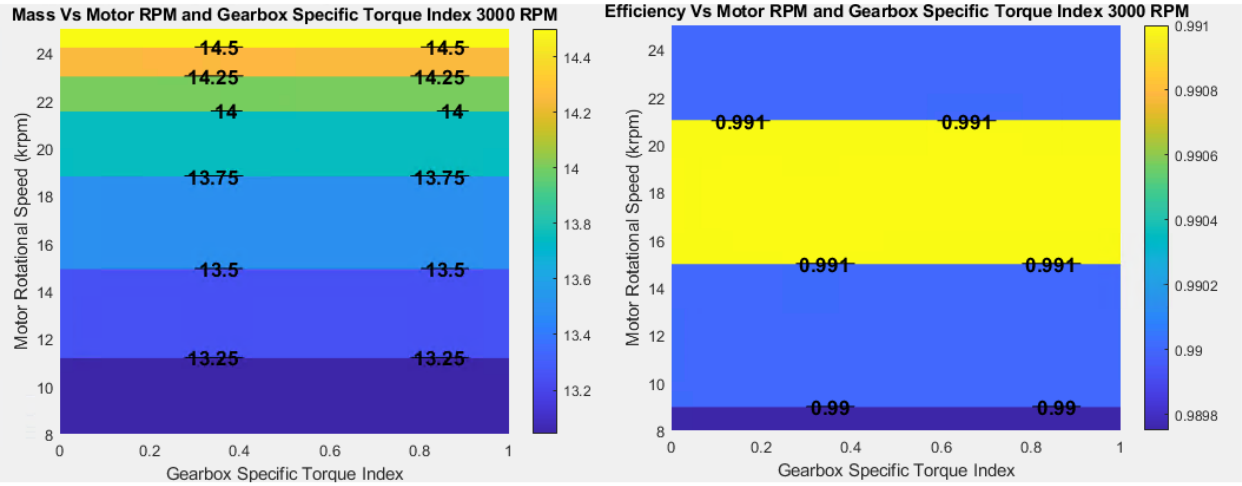

Figure 8 Gearbox scattered interpolant function results for mass and efficiency at 3000 rpm

2. Magnetic Gearboxes.

Second stage magnetic gearbox optimizations were only completed for a 400 RPM propulsor rotor speed assuming an OSMGM on its own, without a second stage CMG, would be optimum at rotor speeds at or above 1000 RPM since optimum concentric magnetic gear (CMG) gear ratio is typically 5 or 6 [18]. CMGs were first optimized for a nominal 1 mm mechanical airgap and a 150% torque margin and then optimized with a 0.5 mm airgap and a 150% torque margin. Appendix B provides the pareto front data at each gear ratio for these optimizations. There is some difficulty in equating mechanical gearboxes designed for a life at peak nominal mission torque and magnetic gearboxes without knowing the required control response for the aircraft and what the absolute maximum required torque is. Here 50% is assumed to be a conservative estimate of what would be required

Figure 9 shows a mass comparison of the lightest magnetic gearboxes with both 1 mm and 0.5 mm airgaps compared to the lightest mechanical gearboxes with 99% efficiency. Magnetic gears are shown to be 10 to 15 kg heavier at a gear ratio of 3 depending on airgap than mechanical gears. The CMGs are shown to increase more significantly in mass with gear ratio then the mechanical gears, but that is in part due to the CMGs only being single stage gearboxes while the mechanical gearboxes are 2 stages above a gear ratio of 5. The 0.5 mm airgap designs increase less significantly in mass with increased gear ratio due to the smaller airgap resulting in less pole-to-pole leakage flux when ring gear pole count gets larger and pole to pole distance gets smaller.

Figures 10 and 11 show the curves used to define second stage magnetic gearbox mass and efficiency at 400 rpm with 1.0 mm and 0.5 mm airgaps. The lightest design at each gear ratio from the data in Appendix B is used assuming magnetic gears need to prioritize mass over their mechanical counterparts to be competitive. At low gear ratios, magnetic gears are shown to be able to achieve efficiencies greater than 99.5% in both Figure 10 and 11 as well as the appendix data at this RPM. This high efficiency is due to the low electrical frequency of the components relative to one another at 400 RPM. Figure 12 shows how efficiency of the CMGs trend with the electrical frequency of the sun gear relative to the ring gear.

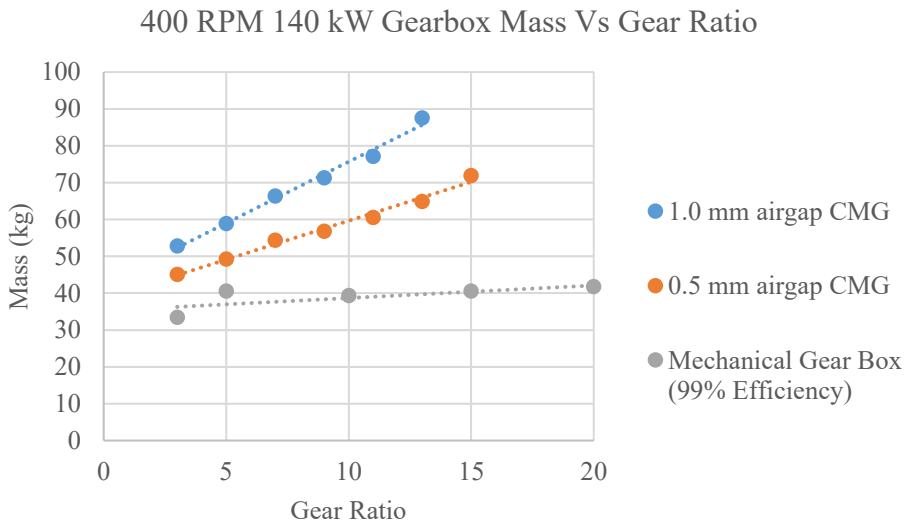

Figure 9 Comparison of magnetic gearbox minimum mass to mechanical gearbox mass with 99% efficiency

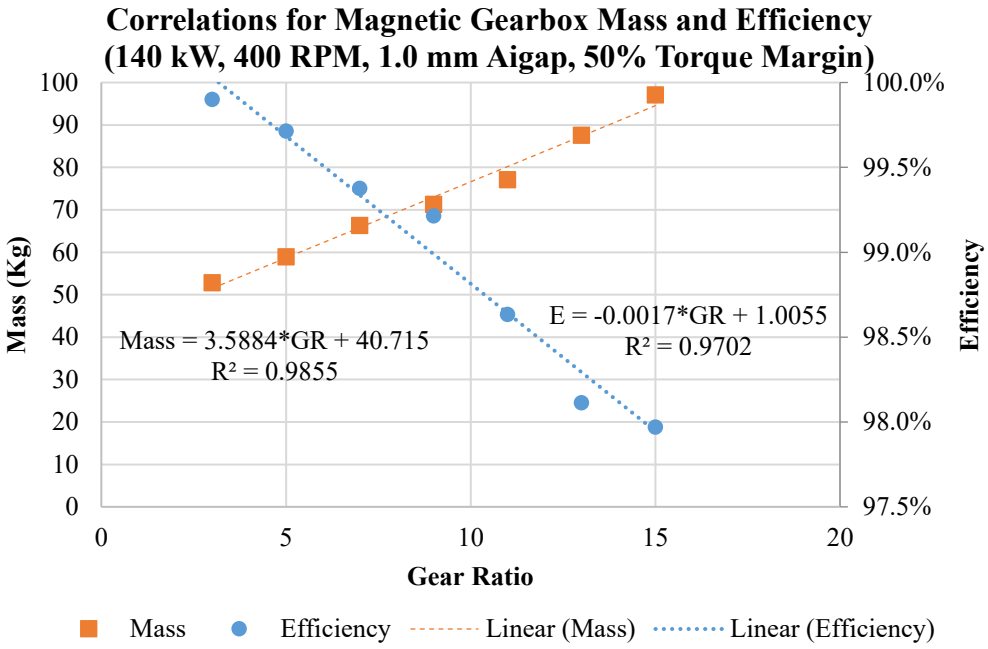

Figure 10 Curves used to define magnetic gearbox mass and efficiency at 140 kW, 400 RPM, 1.0 mm Airgap, and 50% Torque Margin

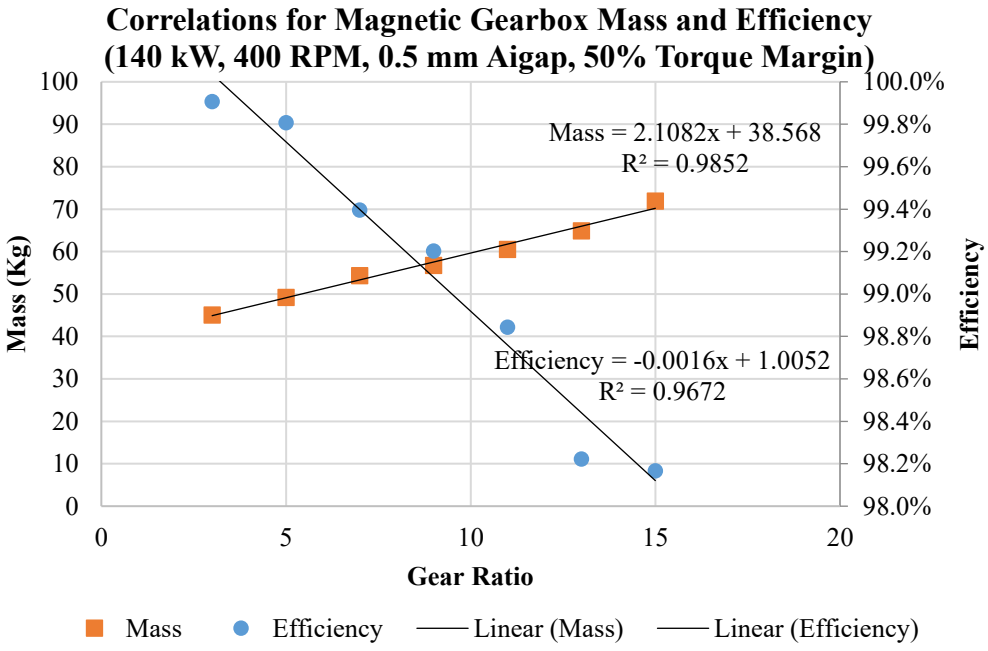

Figure 11 Curves used to define magnetic gearbox mass and efficiency at 140 kW, 400 RPM, 0.5 mm Airgap, and 50% Torque Margin

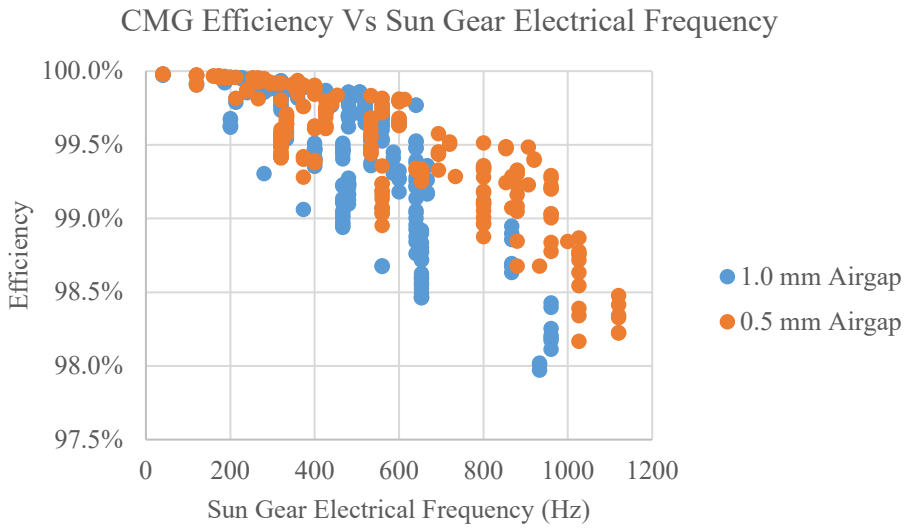

Figure 12 CMG Efficiency Vs Sun Gear Electrical Frequency Relative to the Ring Gear at 140 kW and 400 RPM

B. Drivetrain Comparison

Figures 13 thru 16 show the best design of each topology at 400, 1000, 2000, and 3000 RPM rotor speed. In all cases, the mechanically geared drive is shown to be the lightest. Mechanically geared drivetrains' mass benefit relative to the direct drive and magnetically geared motor topologies is shown to reduce with increased RPM. Figure 17 shows a mass comparison of each drivetrain topology's minimum mass design. Mechanically geared motor drivetrains are shown to have a 30 kg mass benefit at 400 RPM that decays to less than 5 kg at 3000 RPM. All three drives have essentially the same mass at 3000 RPM. This reduction in gearbox benefit with increased rotor RPM trend is primarily the result of gearbox specific torque decaying with reduced torque as shown in the data in Appendix A. Figure 18 shows how overall mechanically geared drivetrain mass primarily trends with the mass of the gearbox for all best designs at all RPM. It also shows that the mass and performance of the other components in the drivetrain (inverter, motor, and TMS) stay roughly constant with changes in rotor RPM as would be suspected. This result verifies that, in the future, only a single full mechanically geared drivetrain study for a given application needs to be completed and then the results can be extrapolated to other rotor RPM's by updating the gearbox mass and efficiency based on reoptimizing the gearbox for different rotor speeds.

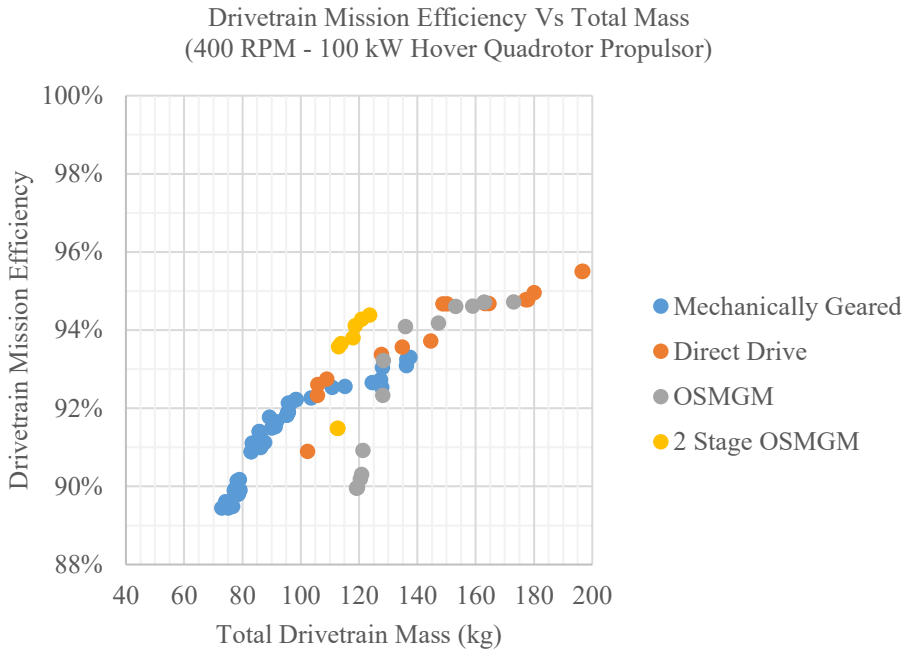

Figure 13 Comparison of different drivetrain topology performances for the mission profile of Table 2 at 400 RPM. Results are reported in terms of total drivetrain mass (TMS + Motor + Gears + Inverter) and drivetrain mission efficiency

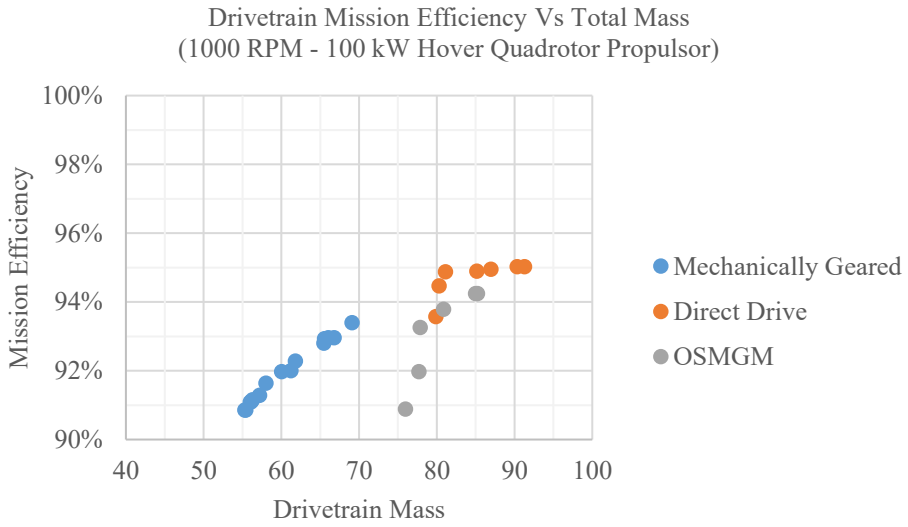

Figure 14 Comparison of different drivetrain topology performances for the mission profile of Table 2 at 1000 RPM. Results are reported in terms of total drivetrain mass (TMS + Motor + Gears + Inverter) and drivetrain mission efficiency

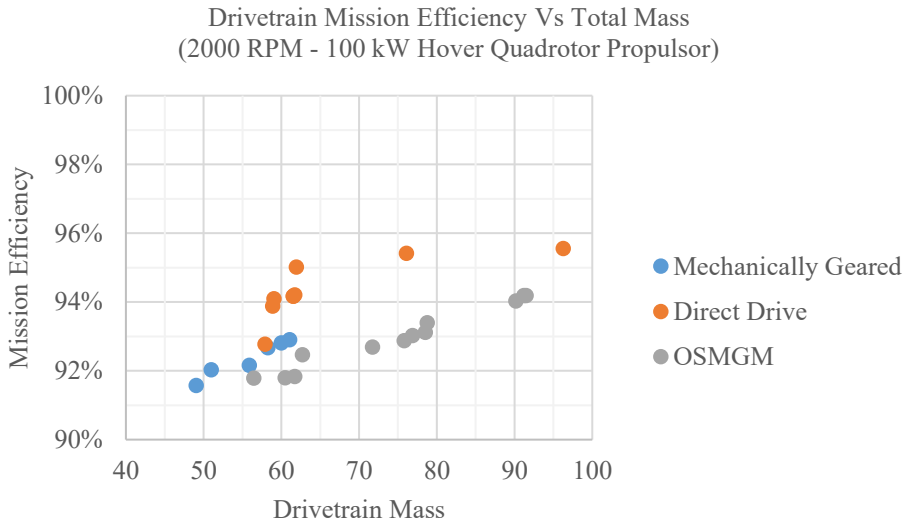

Figure 15 Comparison of different drivetrain topology performances for the mission profile of Table 2 at 2000 RPM. Results are reported in terms of total drivetrain mass (TMS + Motor + Gears + Inverter) and drivetrain mission efficiency

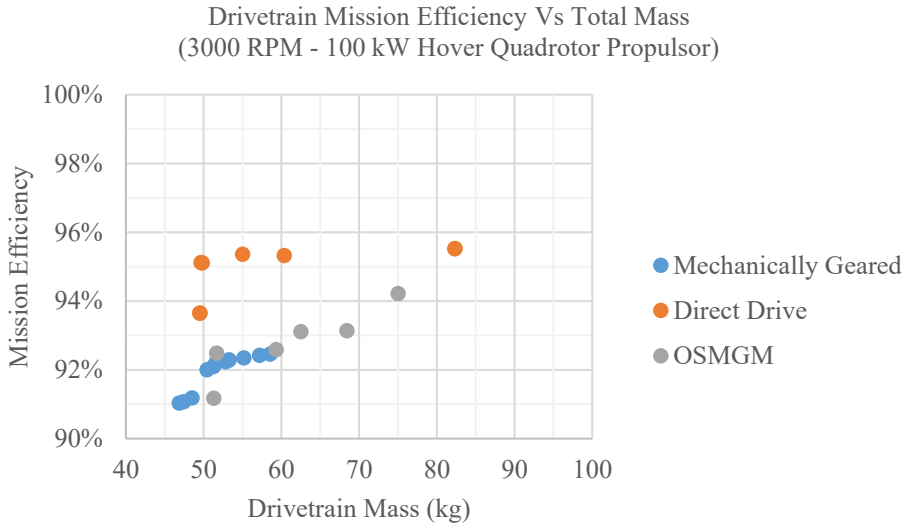

Figure 16 Comparison of different drivetrain topology performances for the mission profile of Table 2 at 3000 RPM. Results are reported in terms of total drivetrain mass (TMS + Motor + Gears + Inverter) and drivetrain mission efficiency

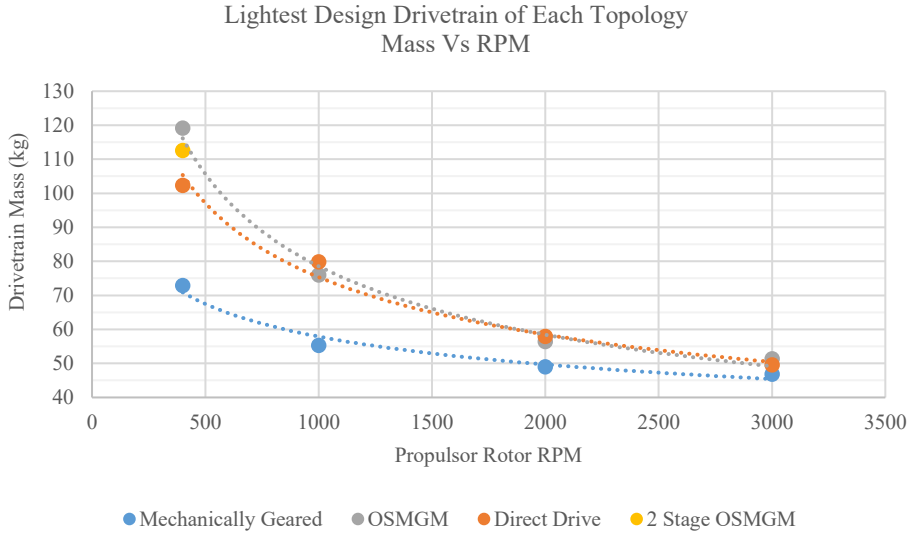

Figure 17 Minimum Mass Drivetrain Mass Vs Propulsor Rotor Speed of Each Drivetrain Topology.

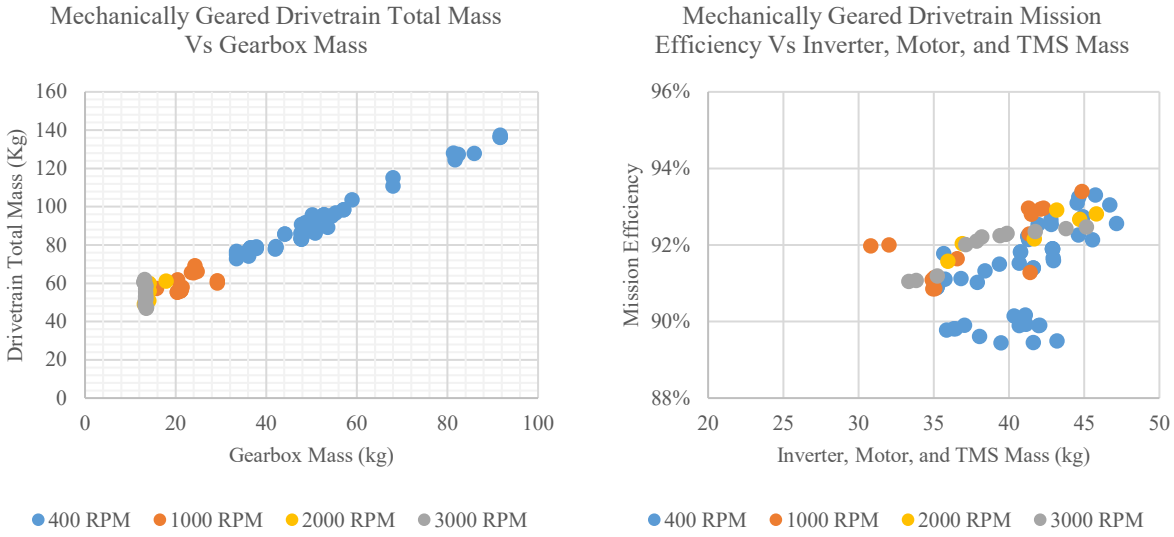

Figure 18 Mechanically geared drivetrain mass dependency on gearbox mass. Left shows trend of total mass vs gearbox mass. Right shows total drivetrain mission efficiency vs the sum of inverter, motor, and TMS mass for mechanically geared drives.

In Figure 13 thru 16, the direct drive drivetrains are generally able to achieve higher efficiency than the mechanically geared and magnetically geared drivetrains. Figure 19 shows the dependance of mission efficiency on the electrical frequency of the motor for all drivetrain pareto front designs. As seen in [7] and [8], electrical frequency is the primary driver of overall drivetrain mission efficiency for the UAM missions. Figure 20 shows that at 400 RPM and at climb condition the geared drivetrain motor and gearbox performance exceeds that of the direct drive motors; however, the direct drive inverters outperform the geared drivetrain inverters at the same condition due to the lower electrical frequencies.

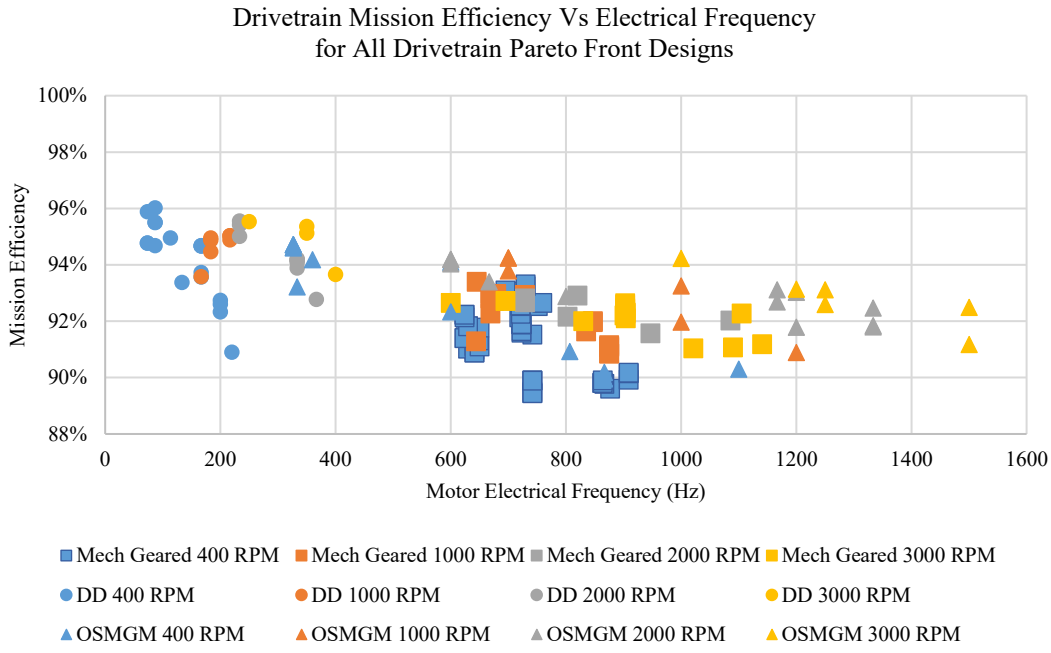

Figure 19 All Pareto Front Drivetrain Designs at every RPM Mission Efficiency Vs Motor Electrical Frequency

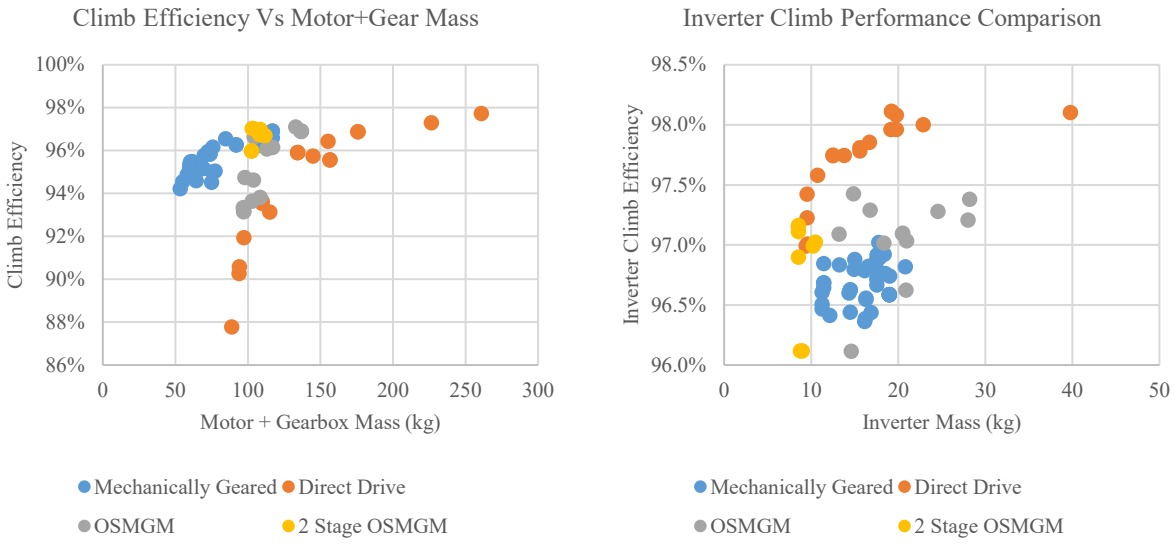

Figure 20 Result of lower electrical frequency at 400 RPM. Left shows that the gear and motor portions of the mechanically and magnetically geared drive trains are able to outperform direct drive at climb conditions. Right shows that the direct drive inverter has appreciably higher efficiency

C. OSMGM Additional Studies

In Figure 13 thru 16 OSMGMs are shown to have minimal mass benefit and worse efficiency than their direct drive counterparts. In past papers [13] [14] [12], it was shown that magnetically geared motors can achieve continuous specific torques greater than their direct counterparts. In this study with the whole drivetrain accounted for, the transient mission profile, and the 50% torque margin on the OSMGM they performed worse. The transient profile allows the direct drive motors to take advantage of the fact that they can boost torque temporarily and use their thermal inertia to not overheat. Magnetically and mechanically geared drives must be sized for full torque and carry the extra

mass and losses corresponding with the additional active mass throughout the mission profile. Additionally, as mentioned above the direct drive case gets appreciable benefits in its inverter by having lower electrical frequency.

Two additional studies were carried out for OSMGMs at 1000 RPM to explore the feasibility of OSMGM's becoming more competitive in the design space. The first study reduced the 50% torque margin for the OSMGM down to 10% corresponding to the required control response torque margin being less than what was estimated in Section III B. The second study left the torque margin the same and reduced airgap to 0.5 mm. 0.5 mm airgaps are feasible in magnetic gears but will have additional manufacturing costs and structural constraints. Figure 21 shows these two studies along with the original 1000 RPM results from Section III B. Both of the two additional studies shift the OSMGM to being directly competitive with the mechanically geared drivetrains for the application. The 0.5 mm airgap results suggest that more refinement of OSMGM geometry could further improve their performance and competitiveness for the application.

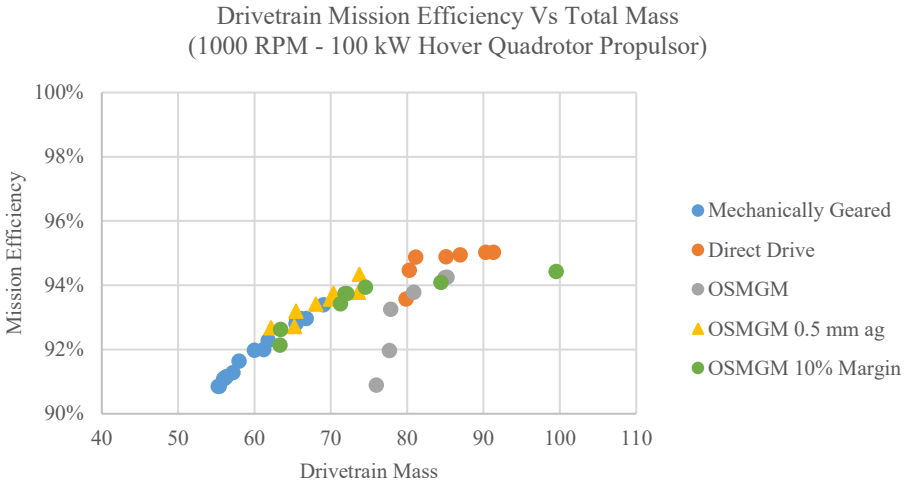

Figure 21 Comparison of different drivetrain topologies performances for the mission profile of Table 2 at 1000 RPM. Results are reported in terms of total drivetrain mass (TMS + Motor + Gears + Inverter) and drivetrain mission efficiency

An additional study was also carried out for a 2 stage OSMGM drive with 0.5 mm airgaps at 400 RPM. The data from Figure 11 was used to define the mass and efficiency of the second stage CMG in the drive. Figure 22 shows the results of this study with the original 400 RPM results. Only a small improvement in 2 stage OSMGM mass is shown. This result is because all pareto optimum 2 stage OSMGM results have second stage gear ratios of 4 or 5. As seen in Figure 9, at these lower gear ratios a 0.5 mm airgap in a CMG only provides a 10 kg benefit over a 1 mm airgap.

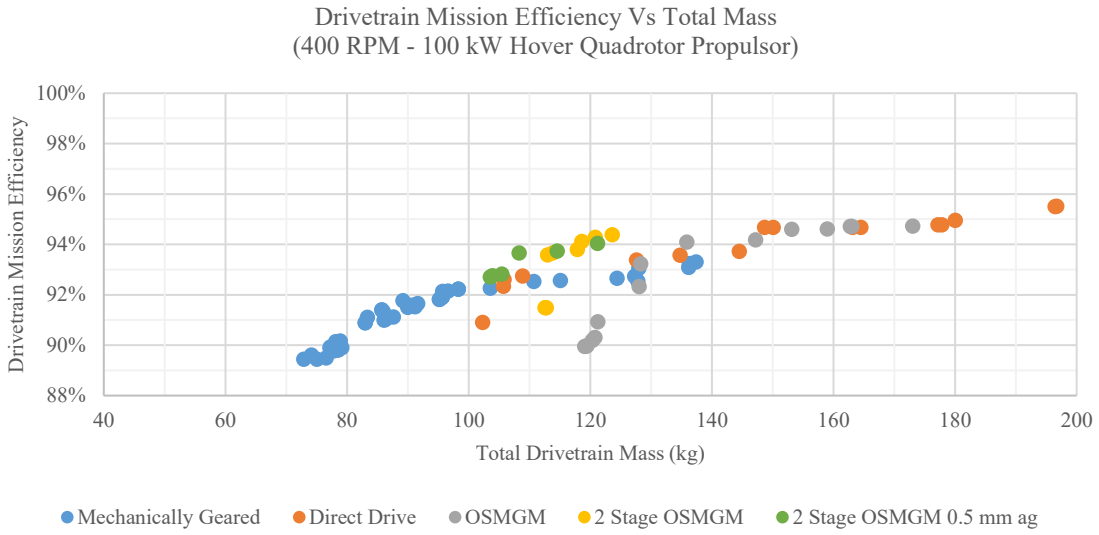

Figure 22 Comparison of different drivetrain topologies performances for the mission profile of Table 2 at 400 RPM. Results are reported in terms of total drivetrain mass (TMS + Motor + Gears + Inverter) and drivetrain mission efficiency

IV. Conclusions and Future Work

In this paper, drivetrain topologies were explored for a 100 kW hover power quadrotor propulsor application. Mechanically geared, direct drive, and magnetically geared drivetrain topologies were compared by optimizing them for a given mission profile at different rotor RPM. Across the design space mechanically geared drives are shown to achieve the lowest mass while direct drive drivetrains achieve the highest efficiencies. The magnetically geared topologies were nominally not competitive in the design space, but that was in large part due to the assumption of a 50% torque margin requirement on nominal mission power for magnetic gears. Reduction of this margin to 10% or the used of 0.5 mm airgaps in the magnetically geared drives did make them competitive in the design space. It should be noted that these studies were completed for a specific power level, a specific application, and with a specific assumed set of technologies and correspondingly do not provide general results that are applicable to all applications and technologies. Future work in this area will:

1. Incorporate reliability models in the design optimization
2. Integration of explicit control response requirements to eliminate torque margin assumptions
3. Expand studies to different applications, technologies, and power levels
4. Explore other possible methods of improving magnetic gear performance beyond just reducing airgap

Appendix

A. Gearbox Preoptimization Results

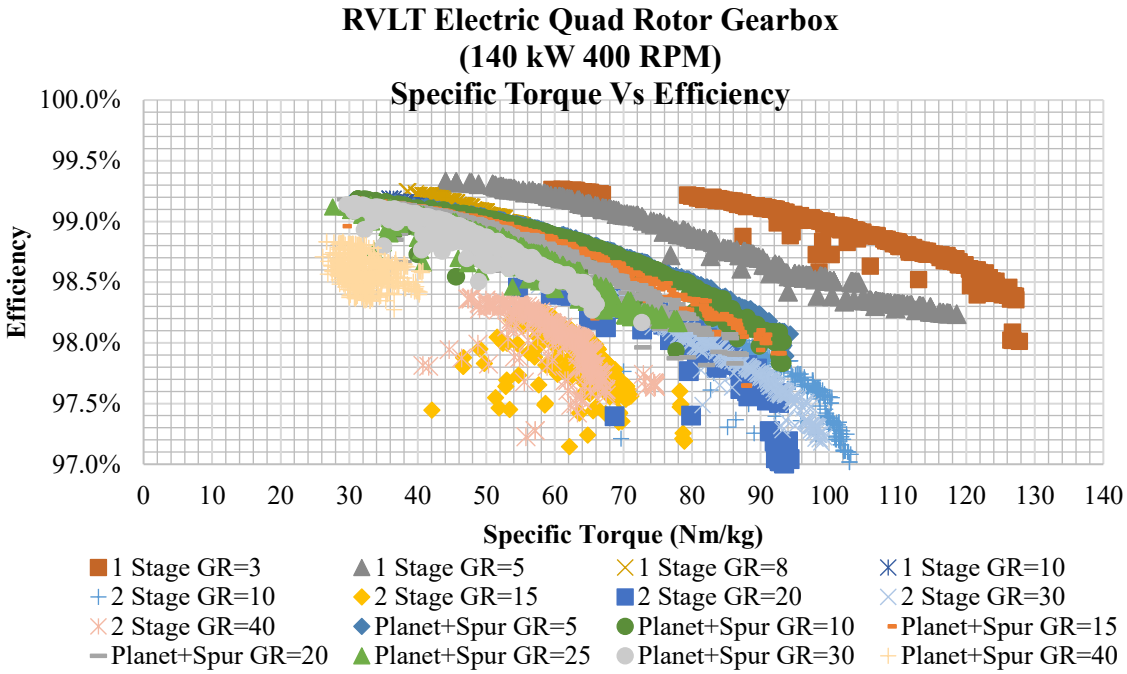

Figure 23 Mechanical Gear Efficiency Vs Specific Torque at 140 kW and 400 RPM

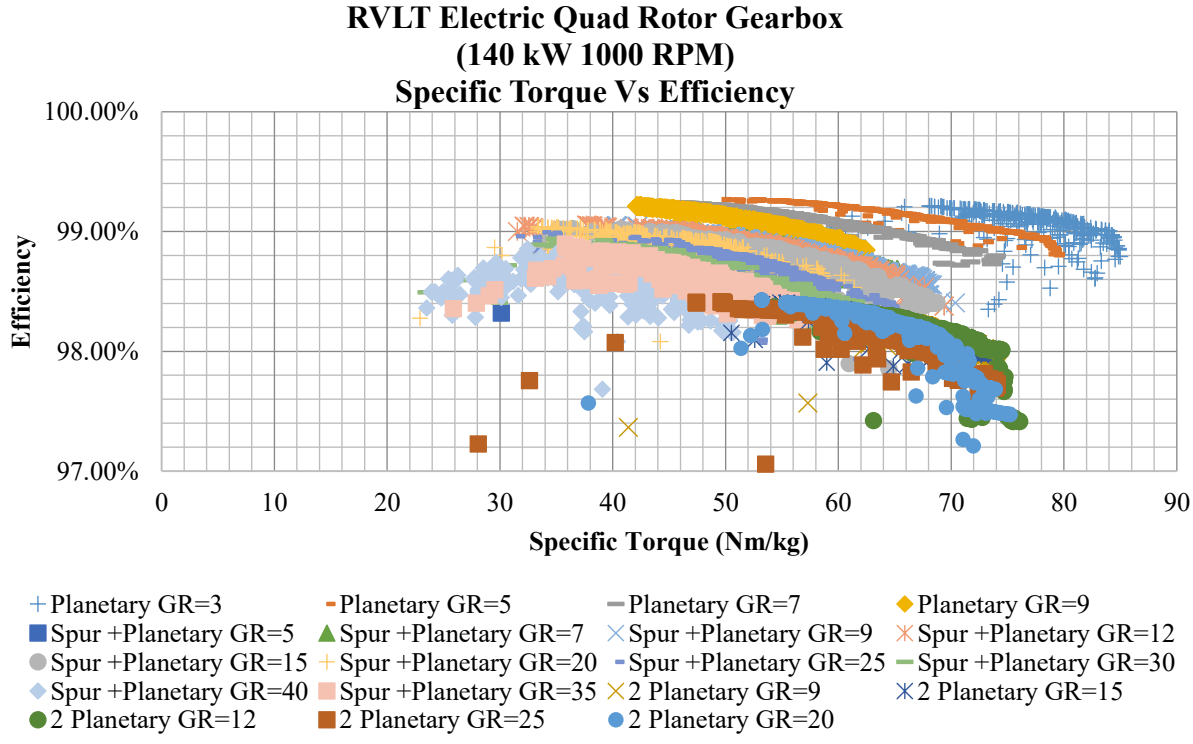

Figure 24 Mechanical Gear Efficiency Vs Specific Torque at 140 kW and 400 RPM

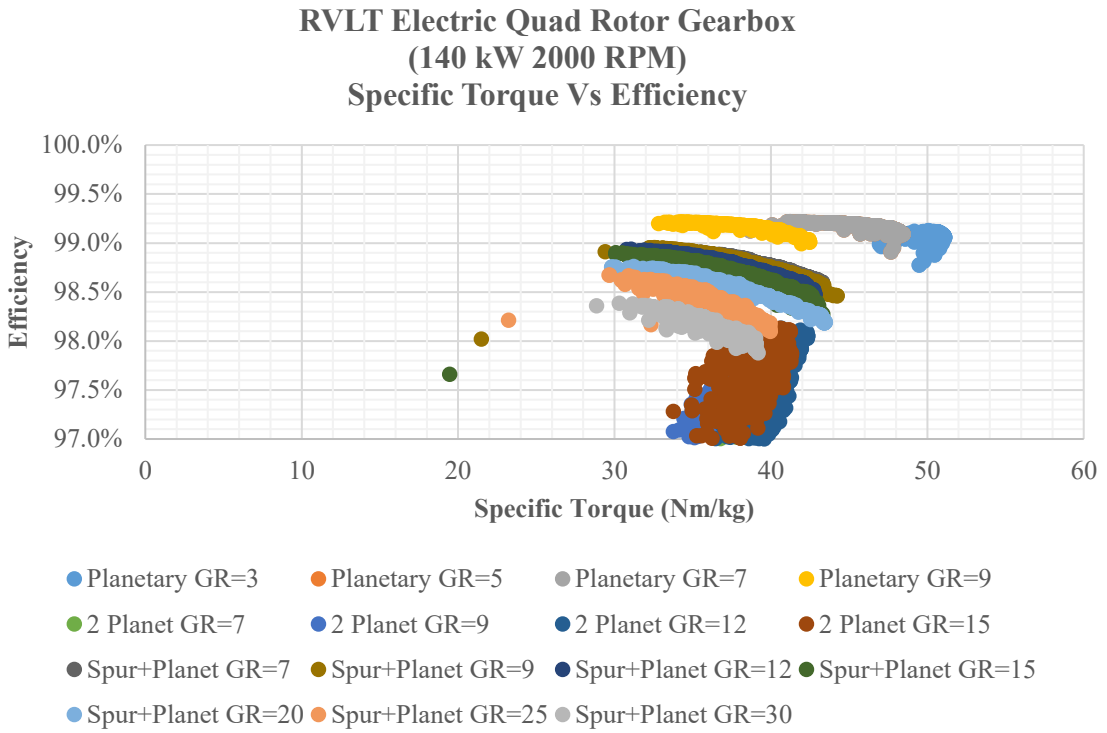

Figure 25 Mechanical Gear Efficiency Vs Specific Torque at 140 kW and 2000 RPM

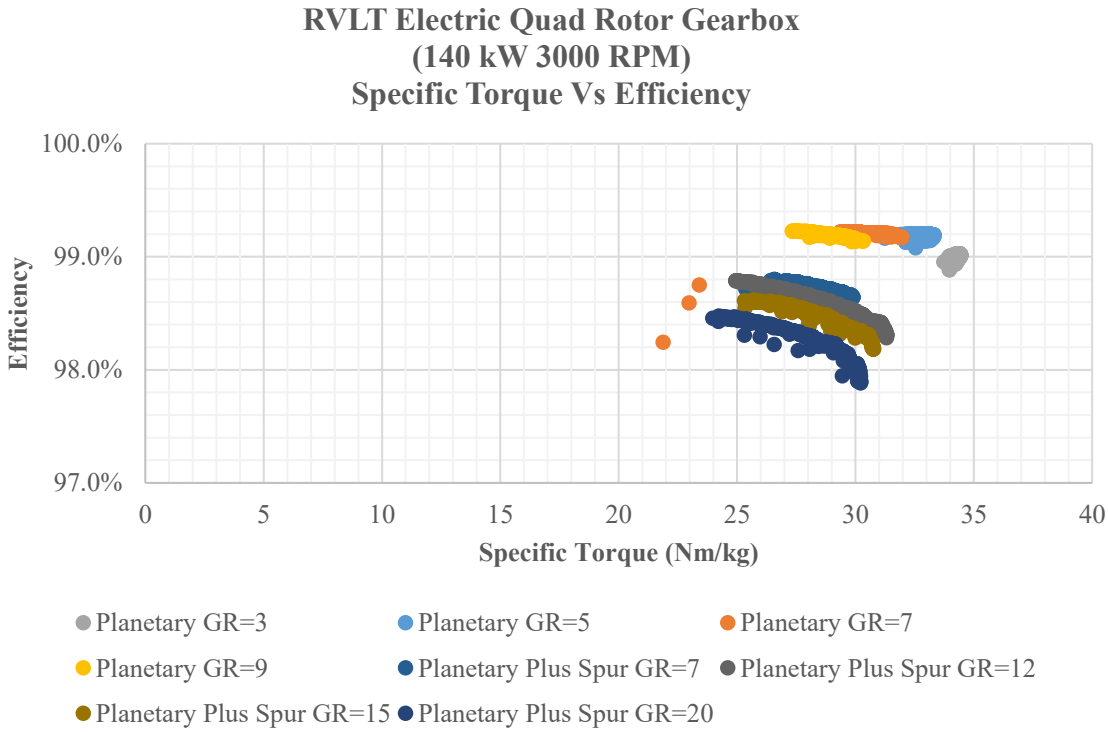

Figure 26 Mechanical Gear Efficiency Vs Specific Torque at 140 kW and 2000 RPM

B. Magnetic Second Stage Gearbox Data

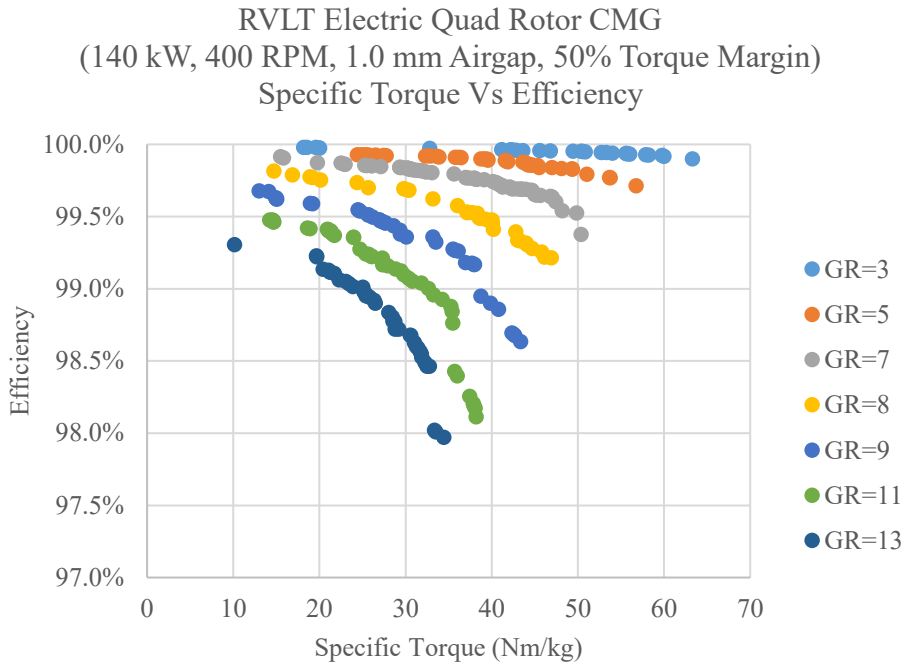

Figure 27 Magnetic Gear Efficiency Vs Specific Torque at 400 RPM, 140 kW, and a 1mm airgap

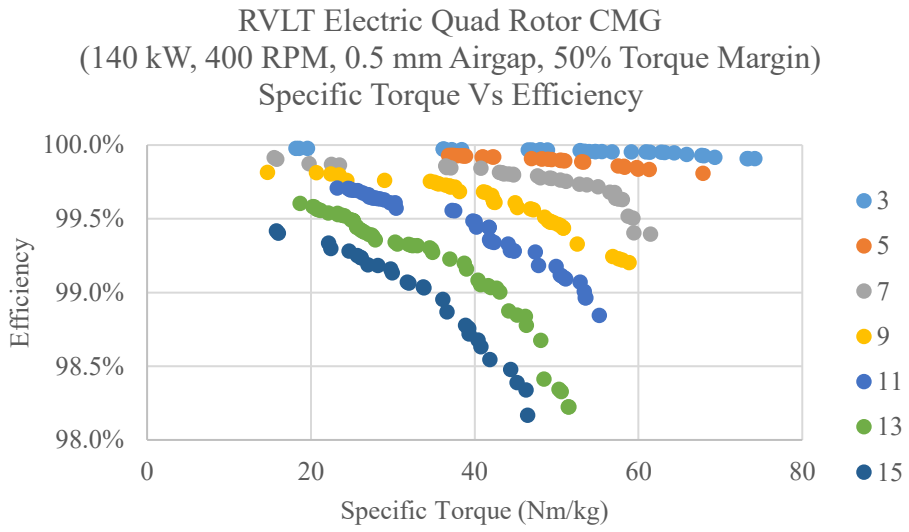

Figure 28 Magnetic Gear Efficiency Vs Specific Torque at 400 RPM, 140 kW, and a 0.5 mm airgap

C. Additional Plots

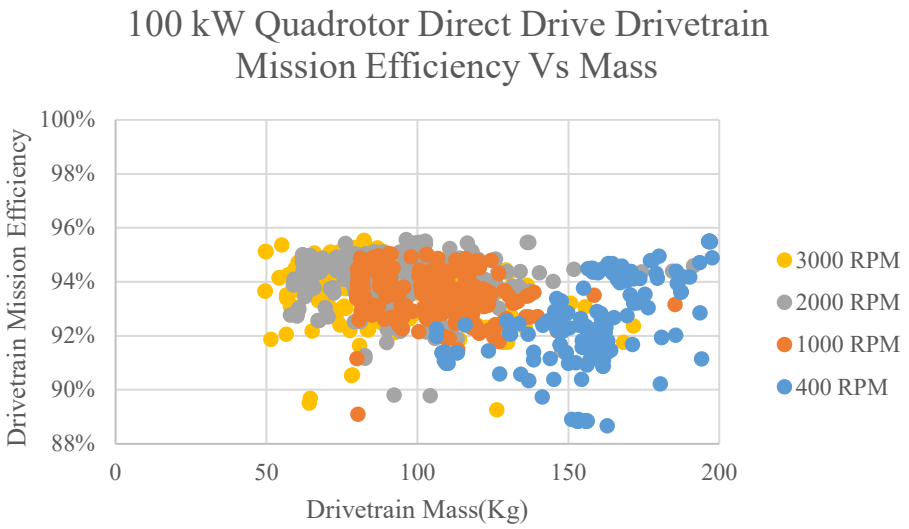

Figure 29 Direct Drive Motor Drivetrain Mission Efficiency Vs Mass at Different Rotor Rotational Speeds

Table 3 Motor and OSMGM Specific Power, Specific Torque, and Efficiency of each lowest mass design

	RPM	Mass	Torque	Specific Torque (Nm/kg)	Specific Power (kW/kg)	Efficiency
Direct Drive Motors	400	88.89	3342	37.60	1.57	96.88%
	1000	69.04	1337	19.36	2.03	96.75%
	2000	38.53	668	17.35	3.63	96.24%
	3000	37.10	446	12.01	3.77	95.79%
Geared Motors	8904	21.65	150	6.94	6.47	96.99%
	9470	19.29	141	7.32	7.26	97.40%
	13125	18.30	102	5.57	7.65	97.56%
	16350	17.82	82	4.59	7.86	97.23%
OSMGM	400	96.99	3342	34.46	1.44	97.09%
	1000	60.29	1337	22.18	2.32	95.63%
	2000	43.33	668	15.43	3.23	96.31%
	3000	39.61	446	11.25	3.53	95.37%
OSMGM 10% Margin	1000	52.17	1337	25.63	2.68	95.75%
OSMGM 0.5mm Airgap	1000	53.17	1337	25.14	2.63	96.65%

Acknowledgments

The authors would like to acknowledge NASA's Revolutionary Vertical Lift Technology Project for sponsoring this work.

V.References

[1] J. Scheidler, V. Asnani and T. Tallerico, "NASA's Magnetic Gearing Research for Electrified Aircraft propulsion," in *AIAA/IEEE Electric Aircraft Technologies Symposium*, Cincinnati, 2018.

[2] M. C. Gardner, B. Praslicka, M. Johnson and H. A. Toliyat, "Optimization of Coaxial Magnetic Gear Design and Magnet Material Grade at Different Temperatures and Gear Ratios," *IEEE Transactions on Energy Conversion,* vol. 36, no. 3, pp. 2493-2501, 2021.

[3] J. Z. Bird, "A Review of Electric Aircraft Drivetrain Motor Technology," *IEEE Transactions on Magnetics,* vol. 58, no. 2, pp. 1-8, 2022.

[4] H. Y. Wong, H. Baninajar, B. Dechant and J. Bird, "Designing a Magnetic Gear for an Electric Aircraft Drivetrain," in *IEEE Energy Conversion Congress and Exposition*, 2020.

[5] A. D. Anderson, N. J. Renner, Y. Wang, D. Lee, S. Agrawal, S. Sirimanna, K. Haran, A. Banerjee, M. Starr and J. Felder, "System Weight Comparison of Electric Machine Topologies for Electric Aircraft Propulsion," in *AIAA/IEEE Electric Aircraft Technologies Symposium*, Cincinnati, 2018.

[6] D. Schweigert, M. Gerlach, A. Hoffmann, B. Morhard, A. Tripps, T. Lohner, M. Otto, B. Ponick and K. Stahl, "On the Impact of Maximum Speed on the Power Density of Electromechanical Powertrains," *Vehicles,* vol. 2, pp. 365-397, 2020.

[7] T. F. Tallerico, J. Chapman and A. D. Smith, "Preliminary Electric Motor Drivetrain Optimization Studies for Urban Air Mobility Vehicles," in *AIAA/IEEE Electric Aircraft Technologies Symposium*, Anaheim, 2022.

[8] T. F. Tallerico, "NASA Reference Motor Designs for Electric Vertical Takeoff and Landing Vehicles," in *AIAA Propulsion and Energy 2021 Forum*, Virtual, 2021.

[9] W. Johnson, C. Silva and E. Solis, "Concept Vehicles for VTOL Air Taxi Operations," in *American Helicopter Society Technical Conferance on Aeromechanics Design for Transfromative Vertical Flight*, San Francisco, 2018.

[10] C. Silva, W. Johnson, K. Antcliff and P. D. Michael, "VTOL Urban Air Mobility Concept Vehicles for Technology Development," in *AIAA Aviation*, Alanta, 2018.

[11] M. Patterson, B. J. German and M. D. Moore, ""Performance and Design of On-Demand Electric Aircraft Concepts"," in *AIAA Aviation Technology, Integration, and Operations Conferance*, Inianapolis, 2012.

[12] T. F. Tallerico, J. J. Scheidler and A. Smith, "Design Study of Double-Sided Axial-Flux Magnetically-Geared Motors for Electric Aircraft Applications," in *AIAA Propulsion and Energy Forum*, Virtual, 2021.

[13] T. F. Tallerico, Z. A. Cameron, J. J. Sheidler and H. Hasseeb, "Outer Stator Magnetically-Geared Motors for Electrified Urban Air Mobility Vehicles," in *AIAA/IEEE Electric Aircraft Technologies Symposium (EATS)*, Virtual, 2020.

[14] T. Tallerico and J. J. Scheidler, "Design Study of a Coupled Inner-Stator Magnetically Geared Motor for Electric Aircraft Applications," in *IEEE Transportation Electrification Conference & Expo (ITEC)*, Anaheim, 2022.

[15] T. F. Tallerico, "Genetic Optimization of Planetary Gearboxes Based on Analytical Gearing Equations," NASA TM-20220008843, Cleveland, 2022.

[16] T. Tallerico and A. D. Smith, "Combined Electromagnetic and Thermal Design Optimization Studies of in-Slot Cooling for UAM Electric Motors," in *IEEE Transportation Electrification Conference & Expo (ITEC)*, Anaheim, 2022.

[17] J. Chapman, H. Hasseeb and S. Schnulo, "Thermal Management System Design for Electrified Aircraft Propulsion Concepts," in *AIAA Propulsion and Energy 2020 Forum*, Virtual, 2020.

[18] T. F. Tallerico, J. J. Scheidler and Z. A. Cameron, "Electromagnetic Mass and Efficiency of Magnetic Gears for Electrified Aircraft," in *AIAA/IEEE Electrified Aircraft Technologies Symposium*, Indinapolis, 2019.

[19] T. F. Tallerico, Z. A. Cameron and J. J. Scheidler, "Design of a Magnetic Gear for NASA's Vertical Lift Quadrotor Concept Vehicle," in *AIAA/IEE Electric Aircraft Technologies Symposium*, Indianapolis, 2019.

[20] S. Gerber and R. J. Wang, "Analysis of the End-Effects in Magnetic Gears and Magnetically Geared Machines," in *Inernational Conferance on Electical Machines Proceedings*, Berlin, 2014.

[21] G. V. Brown, A. F. Kascak, B. Ebihara, D. Johnson, B. Choi, M. Siebert and C. Buccieri, "NASA Glenn Research Center Program in High Power Density Motors for Aeropropulsion," NASA, Cleveland, 2005.